Realization of high-*Q*/*V* photonic crystal cavities defined by an effective Aubry-André-Harper bichromatic potential

A. Simbula,[1] M. Schatzl,[2] L. Zagaglia,[1] F. Alpeggiani,[1,3,4] L. C. Andreani,[1] F. Schäffler,[2] T. Fromherz,[2] M. Galli,[1] and D. Gerace[1,a]
[1]*Department of Physics, University of Pavia, Via Bassi 6, 27100 Pavia, Italy*
[2]*Institute of Semiconductor and Solid State Physics, Johannes Kepler University, Altenberger Str. 69, 4040 Linz, Austria*
[3]*Center for Nanophotonics, FOM Institute AMOLF, Science Park 104, 1098 XG Amsterdam, The Netherlands*
[4]*Department of Quantum Nanoscience, Kavli Institute of Nanoscience, Delft University of Technology, Lorentzweg 1, 2628 CJ Delft, The Netherlands*

(Received 1 December 2016; accepted 22 March 2017; published online 10 April 2017)

We report on the realization of high-*Q*/*V* photonic crystal cavities in thin silicon membranes, with resonances around 1.55 μm wavelength. The cavity designs are based on a recently proposed photonic crystal implementation of the Aubry-André-Harper bichromatic potential, defined from the superposition of two one-dimensional lattices with a non-integer ratio between their periodicity constants. In photonic crystal nanocavities, this confinement mechanism is such that optimized figures of merit can be straightforwardly achieved, in particular an ultra-high-Q factor and diffraction-limited mode volume. Several silicon membrane photonic crystal nanocavities have been realized with measured *Q*-factors in the 1×10^6 range, as evidenced by resonant scattering. The generality of the proposed designs and their easy implementation and scalability make these results particularly interesting for realizing highly performing photonic nanocavities on different material platforms and operational wavelengths. [http://dx.doi.org/10.1063/1.4979708]

The increasing demand for enhanced optical sensitivity in integrated photonic devices has triggered great progress in the design and realization of photonic crystal (PhC) nanocavities, where unprecedented figures of merit have been achieved, such as ultra-high quality factor (Q) and diffraction-limited confinement volumes (V) in the telecom band.[1] In these systems, light-matter interaction can be orders of magnitude larger than in the corresponding bulk medium, allowing to reach the realm of cavity quantum electrodynamics (CQED),[2–4] with potential applications in prospective quantum photonic technologies.[5,6] As recently suggested, nonlinear interactions at the single photon level can also be expected from the intrinsic higher order material response.[7,8] More generally, high Q/V PhC cavities have potential applications in integrated nonlinear photonics,[9,10] light emission,[11–14] and sensing.[15,16]

The design strategies for high Q/V PhC slab cavities have benefited from inspirational analogies with condensed matter systems. After the pioneering demonstration of high Q point defect cavities in a silicon membrane,[17] remarkable Q/V values have been achieved by the local modulation of a PhC waveguide through a shallow trapping potential.[18,19] Following on these ideas, design optimization and nanofabrication advances have allowed further improvement,[20–22] very recently culminating in a record Q value of 11×10^6.[23] Alternatively, inverse-design approaches such as global optimization via genetic algorithms[24] have also proven very effective to achieve experimental Q-factors in excess of 1×10^6.[25]

[a]Electronic address: dario.gerace@unipv.it

Here we report on the realization and optical measurements of high Q/V localized modes in silicon membrane PhC cavities, with operational wavelength around 1.55 μm. Such modes originate from an effective bichromatic potential in a PhC waveguide, which relies on the superposition of two one-dimensional lattices with non-integer ratio between their lattice constants, quantified by the lattice mismatch parameter $\beta = a'/a$, as recently proposed in Ref. 26. This model was originally introduced for the Schrödinger equation to study the localization of massive particles in quasi-periodic lattices, and it is commonly known as the Aubry-André-Harper (AAH) model.[27,28] The AAH bichromatic potential displays a quantum phase transition from extended to localized states as a function of β:[29] when β approaches an irrational value, a transition from Gaussian (also named extended in the literature) to exponentially localized states occurs, which bears similarities with the Anderson localization in purely disordered systems. This transition was first shown in a cold atomic gas,[30] and later in a photonic lattice of one-dimensional ridge waveguides.[31] In the present work, we show for a selected set of rational β values that an effective bichromatic potential can be realized in PhC slabs, too. Remarkably, we are not in the exponential localization regime of the model, and the effective AAH potential naturally leads to a Gaussian envelope of the localized modes over a few lattice sites, which is crucial to achieve ultra-high Q in PhC cavities.[17,32] In fact, we have experimentally measured Q-factors exceeding 1×10^6, essentially limited by fabrication imperfections since the best theoretical values exceed 1×10^9. The mode volume for these localized modes is theoretically estimated as $V \sim (\lambda/n)^3$, pushing the Q/V values of these cavities among the highest demonstrated so far.

The effective AAH bichromatic potential is realized in the present context by starting from a PhC line-defect in a triangular lattice of air holes with periodicity a, the so-called W1 waveguide.[33] Along the axis of W1, a row of air holes with periodicity $a' \neq a$ is introduced, see Fig. 1(a). The radius r' of these air holes is smaller than r, which allows us to increase the fraction of the high-index material. Moreover, the one-dimensional line of reduced air holes is shifted by $\delta = a'/2$ with respect to the original triangular lattice, thus forming a PhC point-defect.

As detailed in Ref. 26, the steady state Maxwell equation for the magnetic field in the PhC structure, $\nabla \times [(1/\varepsilon(\mathbf{r}))\nabla \times \mathbf{H}(\mathbf{r})] = (\omega^2/c^2)\mathbf{H}(\mathbf{r})$ can be approximately recast in a linear eigenvalue problem by expanding the field on a basis of localized states on each site, $\mathbf{H} = \sum c_j \mathbf{H}_j$, where j is an integer labelling the high-index interstitial site along the line-defect with a' periodicity, i.e., corresponding to the positions $x_j = ja'$ with $j = 0, \pm1, \pm2, \ldots$. With this site labelling, $j = 0$ corresponds to the center of the point-defect that will constitute the cavity. For this one-dimensional quasi-periodic lattice, the Maxwell equation can be approximately expressed as $[\omega_0^2 + \Delta\cos(2\pi\beta j)]c_j - J[c_{j-1} + c_{j+1}] = \omega^2 c_j$, where ω_0 is the on-site frequency of the unperturbed lattice, J is the tunnel coupling arising from the overlap of basis functions localized in neighboring interstitial sites, and Δ is the on-site amplitude of the modulation potential. The latter can be approximately recovered graphically, i.e., by comparing the dispersion ω^2 vs. k for two W1 waveguides filled by a row of air holes with

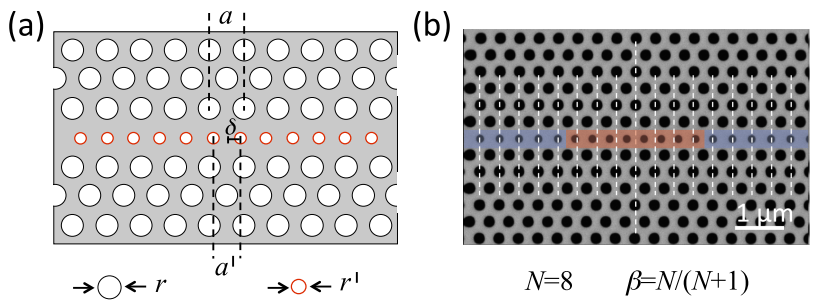

FIG. 1. (a) Schematic picture of a PhC cavity with an effective bichromatic potential: r and a represent the radius and lattice constant of the PhC triangular lattice, while r' and a' represent the radius and lattice constant of the one-dimensional defect lattice, locally shifted by $\delta = a'/2$ with respect to the underlying triangular lattice at the point-defect position. (b) High-resolution top-view SEM image showing a cavity with $N = 8$ and $a = 400$ nm; dashed vertical lines indicate the positions of the original triangular lattice points along the line-defect, highlighting the lattice mismatch defined by $a'/a = \beta = N/(N+1)$, where N represents the number of defect holes with reduced radius. The cavity region is the red-shaded area, while the one-dimensional mirrors closing the cavity along the line-defect are blue-shaded.

reduced radius r', either placed in the original positions of the underlying triangular lattice or shifted by $a/2$ with respect to it.[26] With this identification of parameters, the linear eigenvalue equation above exactly corresponds to the AAH model,[29–31] for which a delocalized-localized quantum phase transition exists on varying Δ/J, and depending on the parameter β.[34] The phase transition exactly occurs at the critical ratio $\Delta/J = 2$ for irrational β, and at larger Δ/J for most rational values of this parameter,[35] such as the ones considered in the following.

To realize the PhC cavities with an effective bichromatic potential and avoiding the formation of replicas in the one-dimensional AAH model, the periodicity a' is only defined for an even number (N) of defect holes along the waveguide, which allows us to keep the cavity symmetric with respect to the center of the defect. The modified lattice constant for the N holes is chosen such that $\beta = N/(N+1)$, hence the lattice points at positions $\pm Na/2 = (N+1)a'/2$ simultaneously belong to both lattices. The PhC cavity is thus formed by N (even number) defect holes of reduced radius $r' < r$ spaced by a', and then continued by holes with radius r' at positions na along the W1 waveguide channel (for every integer $|n| \geq N/2$). A scanning electron microscope (SEM) top-view image of one of the fabricated devices is shown in Fig. 1(b). For this cavity $a' = Na/(N+1) = 356$ nm, while $r = 115$ nm and $r' = 82$ nm ($r'/r \sim 0.7$). We have realized several devices on the same chip, with N ranging from 4 to 24, corresponding to an effective AAH model with a selected set of (rational) β ranging from 0.8 to 0.96.

The fabrication of these PhC cavities was performed on standard silicon-on-insulator (SOI) wafers commercially available from SOITEC (see the supplementary material for details). In the following, we will concentrate on the results obtained for the set of devices with the lattice constant $a = 430$ nm, and nominal $r = 130$ nm, $r' = 90$ nm (again, $r'/r \sim 0.7$). Based on our SEM data, we estimate r and r' to agree within ±3% with the nominal parameters.

The fabricated devices were experimentally tested by cross-polarized resonant scattering.[36] This technique is particularly suited for measuring PhC cavities with ultra-high Q-factors, since it does not rely on evanescent coupling (e.g., through an integrated photonic crystal waveguide or an external fiber taper),[37] thus avoiding any loading effect that may reduce the intrinsic value of the measured Q_{exp}. A scheme of the optical setup is illustrated in Fig. 2(a). A typical spectral response detected from one of our highest Q cavities is shown in Fig. 2(b), displaying $Q_{exp} = 1.2 \times 10^6$ at the resonant wavelength $\lambda \sim 1.56$ μm (see the supplementary material for details).

The experimental Q-factors and cavity mode wavelengths extracted from the resonant scattering spectra are shown in Figs. 3(a) and 3(b) for a series of cavities with different β. The experimental data are compared to full three-dimensional finite-difference time-domain (3D-FDTD) simulations,[38] where all the nominal fabrication parameters of the measured devices were assumed. A very good agreement is found up to $\beta \sim 0.889$ ($N = 8$), both in terms of Q-factor and resonant wavelength. Then, while the measured wavelengths are very well matched by simulations, Q-factors start to

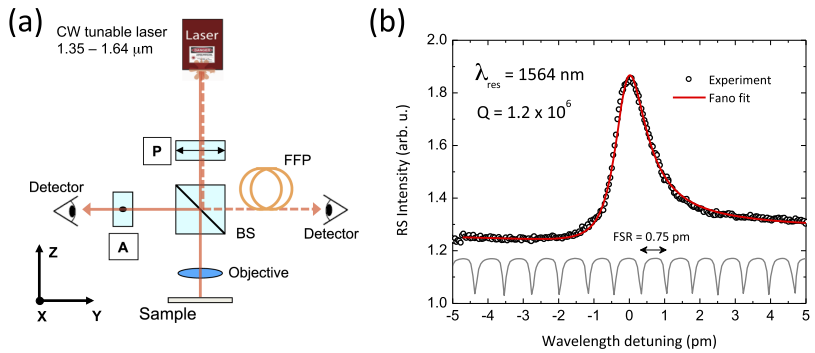

FIG. 2. (a) Schematic illustration of the resonant scattering setup employed to perform the high-resolution spectral detection of the PhC cavity signal in cross-polarization: P is a linear polarizer, A is an orthogonally polarized analyzer, BS an optical beam splitter, and FFP is a fiber-Fabry-Perot interferometer. (b) A typical resonant scattering spectrum measured on one of the high-Q samples (points). The corresponding fit with a Fano-like lineshape is shown with a full line, resulting in the quoted Q-factor and telecom resonant wavelength; the Fabry-Perot spectrum used for wavelength calibration is displayed at the bottom of the plot (grey line), where the corresponding free-spectral range (FSR) is indicated.

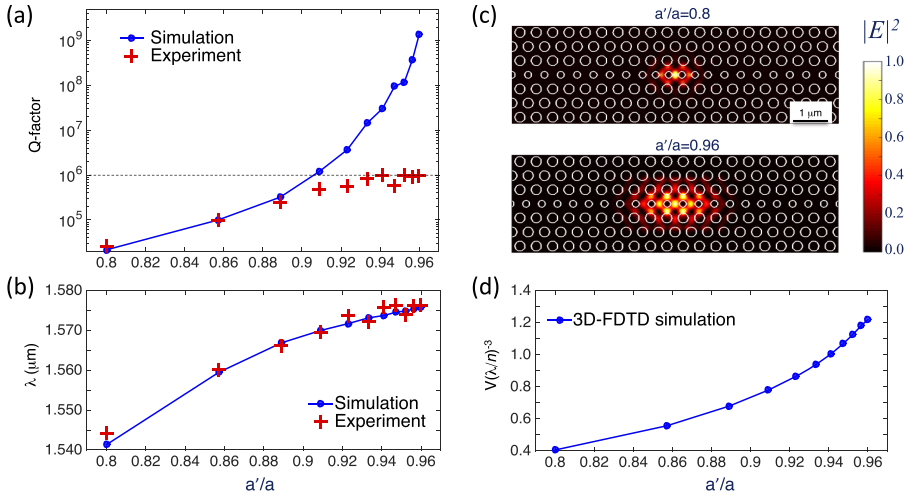

FIG. 3. Experimental and simulated results for cavities with the PhC lattice constant a = 430 nm and nominal radii r = 130 nm, r' = 90 nm: (a) Quality factor as a function of the AAH lattice mismatch parameter, (b) corresponding resonant wavelength, as measured from the resonant scattering spectra. The 3D-FDTD calculated Q and λ are shown for a direct comparison; the dashed line indicates the $Q = 1 \times 10^6$ threshold. (c) Simulated electric field intensity profiles for the shortest and longest cavities (N = 4 and N = 24, respectively), represented in a color scale contour plot; in both cases, the intensities have been normalized to the peak values at the cavity antinodes. (d) Calculated cavity mode volumes as a function of β.

deviate and roughly saturate to $Q_{exp} \sim 10^6$. The theoretical Qs increase up to values well exceeding $Q_{theo} = 10^9$ at $\beta = 0.96$ (N = 24), as already reported.[26] The extremely large Q_{theo}-values can be understood by fitting the AAH model parameters suitable for the present devices, which we have determined as $\Delta = 0.008\,05(a/2\pi c)^2$ and $J = 0.007\,15(a/2\pi c)^2$, respectively. Hence, the value $\Delta/J \sim 1.125$ automatically yields a Gaussian localization regime for $\beta < 1$, the critical value for the transition to exponential localization of the field being at least $\Delta/J = 2$.[28,29,35] As it is accepted in the PhC cavity literature, a perfectly Gaussian envelope is a favorable condition to achieve ultra-high Q-factors in PhC slab cavities.[17,32] In the bichromatic PhC cavity designs such ultra-high Q condition is naturally met, depending on a single design parameter (β), and without the need for extensive numerical simulations (see supplementary material for details). For $\beta > 0.9$, the deviation of the measured Q-factors from the theoretical ones can be mainly attributed to the role of fabrication imperfections. In fact, the experimental values can be expressed as $Q_{exp}^{-1} = Q_{theo}^{-1} + Q_{ext}^{-1}$, where Q_{ext} is the Q-factor determined by extrinsic losses introduced in the fabrication process, such as disorder and roughness of the lower PhC membrane surface exposed to the 40% HF etch during SiO_2 removal, as well as material absorption.[39,40] In the present samples, it can be inferred that the limiting Q-factor induced by extrinsic losses is on the order of $Q_{ext} \sim 10^6$, which makes Q_{exp} saturate at such values even when Q_{theo} is orders of magnitude larger. A detailed study on the role of disorder in these PhC cavities, as well as a systematic comparison with alternative designs along the lines reported, e.g., in Ref. 41, is beyond the scope of the present manuscript.

The mode volume of PhC cavities can be directly calculated from the steady state electric-field profile of the localized modes simulated by 3D-FDTD. As examples, we show in Fig. 3(c) the mode profiles for the smallest ($\beta = 0.8$, or N = 4) and the largest ($\beta = 0.96$, or N = 24) cavity considered in this work, respectively. The spatial extension of the mode increases with β. To give a quantitative estimate, the mode volume can be estimated from the usual CQED definition, $V = \int d\mathbf{r}\, \varepsilon(\mathbf{r})|E(\mathbf{r})|^2 / \max\{\varepsilon(\mathbf{r})|E(\mathbf{r})|^2\}$, for a single emitter located at the electric field intensity maximum (i.e., the cavity center here).[1,42] The mode volumes calculated for the experimentally characterized cavities are shown in Fig. 3(d) in units of $(\lambda/n)^3$, where λ is the resonant wavelength of each cavity and n = 3.5 is the Si refractive index. The mode volume remains of the order of the diffraction limit even for the largest cavities, ranging from 0.034 μm^3 and 0.11 μm^3 in real units. In particular, for $\beta = 0.96$, the theoretical $Q_{theo}/V \sim 1.5 \times 10^9 (\lambda/n)^{-3}$ ratio is among the largest ever reported for 2D PhC slab cavities, competing in particular with the highest $Q_{theo}/V \sim 2.5 \times 10^9 (\lambda/n)^{-3}$

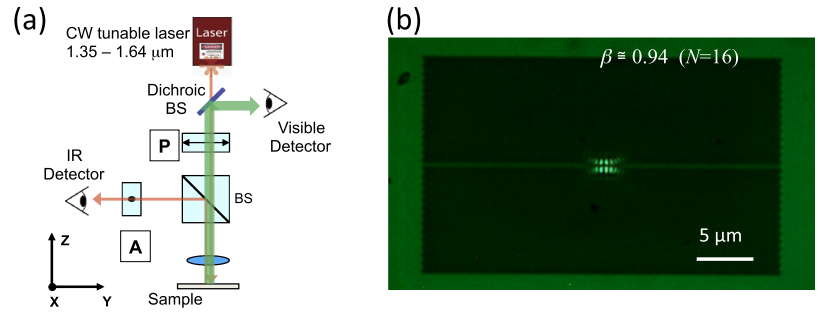

FIG. 4. (a) Schematic representation of the modified setup allowing to image (in the visible) the TH signal emitted from the cavity excited at the resonant wavelength (in the near-infrared), and (b) typical green TH light emission from one of the fabricated samples (in this case, $N = 16$), showing the localized nature of the cavity mode in a diffraction-limited spot.

design.[43] If we relate the theoretical mode volumes to the measured Q-factors, we see that the largest value is obtained for the devices corresponding to $\beta \simeq 0.941$ ($N = 16$) and $\beta \simeq 0.952$ ($N = 20$), which display a remarkable $Q_{exp}/V \sim 10^6(\lambda/n)^{-3}$, i.e., comparable to our previous reports,[25] and not far from the recently achieved record value $\sim 7 \cdot 10^6(\lambda/n)^{-3}$ in optimized heterostructure PhC cavities.[23] For the latter, we further notice that ultra-high theoretical $Q \sim 10^8$ and mode volume $V \sim 1.4(\lambda/n)^3$ require at least three independent design parameters plus ultra-fine (i.e., sub-nanometer) nearby holes optimization. In contrast, our cavities readily attain theoretical Q-factors up to 10^9 with a single design parameter, which can be set with a very large tolerance of about 2% (i.e., as large as 9 nm for a lattice constant $a = 430$ nm). Indeed, as shown in Figs. 3(a) and 3(d), for $r' \simeq 0.7r$ any value of a'/a between 0.94 and 0.96 yields a theoretical $Q > 10^8$ with a mode volume $V < 1.2(\lambda/n)^3$.

Finally, we report in Fig. 4 the results of a nonlinear optical experiment performed on a slightly modified setup, schematically illustrated in Fig. 4(a), which allows to record the higher-order harmonic emission from the sample. The selected PhC cavity device is resonantly excited with a continuous wave (cw) laser at the localized mode wavelength, and the nonlinear light emission is collected and imaged with a detector in the visible range (in this case, a commercially available Nikon camera). As an example, we show in Fig. 4(b) the green light emission from a $\beta \simeq 0.94$ ($N = 16$) cavity, excited at a resonant wavelength of $\lambda = 1563$ nm, and thus emitting in the third harmonic (TH) at $\lambda_{TH} = 521$ nm, which gives the green signal. We notice that the TH is generated by the bulk $\chi^{(3)}$ susceptibility of silicon, which is strongly enhanced by the confinement of the cavity mode in a $V \sim (\lambda/n)^3$ effective volume, and it thus allows us to detect the nonlinear signal even under cw excitation, as already shown previously.[44] Notice also that the measured TH emitted power is of the order of 1 pW for about 10 μW coupled power into the cavity, which results in a net $\sim 10^{-7}$ TH generation efficiency.[45] To the purposes of the present work, the TH image of Fig. 4 gives a direct evidence of the Gaussian localization of the resonant modes in the PhC cavities with an effective bichromatic potential.

In conclusion, these devices are particularly promising for the straightforward realization of highly tolerant, highly performing photonic crystal cavities, potentially useful for a number of applications in integrated nonlinear photonics, light emission, and sensing, since they do not require any sophisticated design strategy or time-consuming numerical simulations, but the tuning of a single parameter like the lattice mismatch.

See supplementary material for the details regarding (a) the fabrication process, (b) the experimental techniques employed and the corresponding data analysis, (c) the discussion on the relevant design parameters for the photonic crystal cavities with an effective Aubry-André-Harper bichromatic potential allowing to reach ultra-high theoretical Q-factor values.

[1] M. Notomi, Rep. Prog. Phys. **73**, 096501 (2010).
[2] K. Hennessy, A. Badolato, M. Winger, D. Gerace, M. Atatüre, S. Gulde, S. Fält, E. Hu, and A. Imamoğlu, Nature **445**, 896 (2007).
[3] A. Faraon, I. Fushman, D. Englund, N. Stoltz, P. Petroff, and J. Vučković, Nat. Phys. **4**, 859 (2008).
[4] A. Reinhard, T. Volz, M. Winger, A. Badolato, K. J. Hennessy, E. L. Hu, and A. Imamoğlu, Nat. Photonics **6**, 93 (2012).
[5] J. L. O'Brien, A. Furusawa, and J. Vučković, Nat. Photonics **3**, 687 (2009).

[6] D. Gerace, H. E. Türeci, A. Imamoğlu, V. Giovannetti, and R. Fazio, Nat. Phys. **5**, 281 (2009).
[7] S. Ferretti and D. Gerace, Phys. Rev. B **85**, 033303 (2012).
[8] A. Majumdar and D. Gerace, Phys. Rev. B **87**, 235319 (2013).
[9] M. Notomi, A. Shinya, S. Mitsugi, G. Kira, E. Kuramochi, and T. Tanabe, Opt. Express **13**, 2678 (2005).
[10] S. Combrié, A. De Rossi, Q. V. Tran, and H. Benisty, Opt. Lett. **33**, 1908 (2008).
[11] S. Strauf, K. Hennessy, M. T. Rakher, Y.-S. Choi, A. Badolato, L. C. Andreani, E. L. Hu, P. M. Petroff, and D. Bouwmeester, Phys. Rev. Lett. **96**, 127404 (2006).
[12] M. Nomura, N. Kumagai, S. Iwamoto, Y. Ota, and Y. Arakawa, Nat. Phys. **6**, 1518 (2010).
[13] B. Ellis, M. A. Mayer, G. Shambat, T. Sarmiento, J. Harris, E. E. Haller, and J. Vučković, Nat. Photonics **5**, 297 (2011).
[14] A. Shakoor, R. Lo Savio, P. Cardile, S. L. Portalupi, D. Gerace, K. Welna, S. Boninelli, G. Franzò, F. Priolo, T. F. Krauss, M. Galli, and L. O'Faolain, Laser Photonics Rev. **7**, 114 (2013).
[15] S.-H. Kwon, T. Sünner, M. Kamp, and A. Forchel, Opt. Express **16**, 11709 (2008).
[16] J. Jágerská, H. Zhang, Z. Diao, N. Le Thomas, and R. Houdré, Opt. Lett. **35**, 2523 (2010).
[17] Y. Akahane, T. Asano, B.-S. Song, and S. Noda, Nature **425**, 944 (2003).
[18] B.-S. Song, S. Noda, T. Asano, and Y. Akahane, Nat. Mater. **4**, 207 (2005).
[19] E. Kuramochi, M. Notomi, S. Mitsugi, A. Shinya, T. Tanabe, and T. Watanabe, Appl. Phys. Lett. **88**, 041112 (2006).
[20] T. Tanabe, M. Notomi, E. Kuramochi, A. Shinya, and H. Taniyama, Nat. Photonics **1**, 49–52 (2007).
[21] Y. Taguchi, Y. Takahashi, Y. Sato, T. Asano, and S. Noda, Opt. Express **19**, 11916–11921 (2011).
[22] H. Sekoguchi, Y. Takahashi, T. Asano, and S. Noda, Opt. Express **22**, 916–924 (2014).
[23] T. Asano, Y. Ochi, Y. Takahashi, K. Kishimoto, and S. Noda, Opt. Express **25**, 1769–1777 (2017).
[24] M. Minkov and V. Savona, Sci. Rep. **4**, 5124 (2014).
[25] Y. Lai, S. Pirotta, G. Urbinati, D. Gerace, M. Minkov, V. Savona, A. Badolato, and M. Galli, Appl. Phys. Lett. **104**, 241101 (2014).
[26] F. Alpeggiani, L. C. Andreani, and D. Gerace, Appl. Phys. Lett. **107**, 261110 (2015).
[27] P. G. Harper, Proc. Phys. Soc., Sect. A **68**, 874 (1955).
[28] S. Aubry and G. André, Ann. Isr. Phys. Soc. **3**, 133 (1980).
[29] M. Modugno, New J. Phys. **11**, 033023 (2009).
[30] G. Roati, C. D'Errico, L. Fallani, M. Fattori, C. Fort, M. Zaccanti, G. Modugno, M. Modugno, and M. Inguscio, Nature **453**, 895 (2008).
[31] Y. Lahini, R. Pugatch, F. Pozzi, M. Sorel, R. Morandotti, N. Davidson, and Y. Silberberg, Phys. Rev. Lett. **103**, 013901 (2009).
[32] D. Englund, I. Fushman, and J. Vuçković, Opt. Express **13**, 5961 (2005).
[33] J. D. Joannopoulos, S. G. Johnson, J. N. Winn, and R. D. Meade, *Photonic Crystals: Molding the Flow of Light* (Kluwer Academic, Boston, 2008).
[34] In comparing the photonic AAH model to the original one, notice that the solutions of the eigenvalue equation are frequencies squared, and not the eigenenergies. Hence, also J and Δ have dimensions of ω^2.
[35] S. Y. Jitomirskaya, Ann. Math. **150**, 1159 (1999).
[36] M. Galli, S. L. Portalupi, M. Belotti, L. C. Andreani, L. O'Faolain, and T. F. Krauss, Appl. Phys. Lett. **94**, 071101 (2009).
[37] M. McCutcheon, G. W. Rieger, I. W. Cheung, J. F. Young, D. Dalacu, S. Frédéric, P. J. Poole, G. C. Aers, and R. Williams, Appl. Phys. Lett. **87**, 221110 (2009).
[38] We employed a commercial software from Lumerical Solutions, http://www.lumerical.com/tcad-products/fdtd/. For the simulations shown in the present work, Q-factors are determined to within a percent error; for $Q_{theo} > 10^8$, the reported values might be a lower bound, limited by finite size effects and discretization errors introduced by the FDTD simulation.
[39] D. Gerace and L. C. Andreani, Photonics Nanostruct. Fundam. Appl. **3**, 120 (2005).
[40] S. L. Portalupi, M. Galli, M. Belotti, L. C. Andreani, T. F. Krauss, and L. O'Faolain, Phys. Rev. B **84**, 045423 (2011).
[41] K. Welna, S. L. Portalupi, M. Galli, L. O'Faolain, and T. F. Krauss, IEEE J. Quantum Electron. **48**, 1177–1183 (2012).
[42] L. C. Andreani, G. Panzarini, and J.-M. Gérard, Phys. Rev. B **60**, 13276 (1999).
[43] M. Notomi and H. Taniyama, Opt. Express **16**, 18657 (2008).
[44] M. Galli, D. Gerace, K. Welna, T. F. Krauss, L. O'Faolain, G. Guizzetti, and L. C. Andreani, Opt. Express **18**, 26613 (2010).
[45] This value is about one order of magnitude better than what was reported in Ref. 44, which is consistent with the scaling of the TH efficiency in terms of Q-factor and coupling efficiency. In fact, the TH conversion efficiency scales as the third power of the product ηQ, where η represents the coupling efficiency of the pump to the cavity mode at the fundamental resonant frequency. In the present case, while the Q-factor of these cavities is much larger than those measured in Ref. 44, the vertical coupling efficiency is much lower, resulting in a comparable TH emission power.